Arch Appl Mech (2013) 83:783–798
DOI 10.1007/s00419-012-0717-2

ORIGINAL

R. Ramezanpour · M. Ghayour · S. Ziaei-Rad

A novel method for slant crack detection in rotors based on turning in two directions

Received: 26 July 2012 / Accepted: 1 November 2012 / Published online: 20 November 2012
© Springer-Verlag Berlin Heidelberg 2012

Abstract This paper presents a novel way to detect fatigue slant cracks in rotors based on theoretical discussion. Hence, the dynamic behaviour of a Jeffcott rotor system with a mid-span slant crack under arbitrary crack orientations is studied. First, using concepts of fracture mechanics, the flexibility matrix and subsequently the system's stiffness matrix are calculated. A symmetric relation for a global stiffness matrix is presented and proved. Next, the motion equations of the system that are obtained in four directions, two transverse, one torsional and one longitudinal, are solved using the Runge–Kutta numerical method. The characteristics of crack orientations for angles greater than 90° (transverse crack) are investigated in detail and their influence on the elements of the crack compliance matrix is presented. Also, slant crack characteristics with complementary angles are compared to each other. It is shown that the difference between cracked systems with complementary angles is only in 3rd row (3rd column) of the crack compliance matrix, and also it is shown that due to the presence of a slant crack, the system responses in forward and backward motion are different. Using the frequency responses of the shaft obtained, a technique to detect the existence of slant cracks on the shaft was proposed. This novel method is a simple way that can be used for slant crack detection in rotors.

Keywords Rotor system · Slant crack · Complementary crack angles · Backward and forward whirl

1 Introduction

Modern day rotors are designed to achieve high-speed revolution. On the other hand, such systems have a significant mass and thus considerable energy. It is obvious that any phenomenon that causes the sudden release of this energy may lead to a catastrophic failure in such systems. Since the 1980s, numerous researchers have studied the response of rotating systems with cracks. Many vibration-based techniques have also been used to diagnose the existence of cracks in simple engineering structures such as beams, trusses and rotors. These techniques are based on the changes in the vibration response or vibration characteristics of the systems. As of the 1970s, many works have been carried out in this field that have been well documented by Dimarogonas [1] and Wauer [2].

Much of the research has been focused on rotors with one or two transverse cracks. Papadopoulos et al. [3] investigated the coupling of the longitudinal and bending vibrations of a rotating shaft, due to an open

R. Ramezanpour (✉) · M. Ghayour · S. Ziaei-Rad
Department of Mechanical Engineering, Isfahan University of Technology, 84156-83111 Isfahan, Iran
E-mail: r.ramezanpour.k@me.iut.ac.ir

M. Ghayour
E-mail: ghayour@cc.iut.ac.ir

S. Ziaei-Rad
E-mail: szrad@cc.iut.ac.ir

transverse crack. They obtained local flexibility due to the presence of the crack by a 6×6 matrix and concluded that damped and un-damped free and forced coupled vibration between longitudinal and bending vibration due to a crack is a very useful property, which introduces a basis for crack identification in rotating shafts. Sekhar [4] investigated the dynamic behaviour of a cracked rotor, in particular that of a rotor with two open transverse cracks. Darpe et al. [5] investigated a simple Jeffcott rotor with two transverse surface cracks. However, he assumed that one crack remains open while another is breathing. Also, the effect of the interaction of two cracks on breathing behaviour and on the unbalance response of a rotor has been studied. Darpe et al. [6] proposed a response-dependent nonlinear breathing crack model. Considering all six degrees of freedom per node, the stiffness matrix for a Timoshenko beam element is modified to account for the effect of the crack. Using this model, they studied coupling between longitudinal, lateral and torsional vibrations. Analyses of transient response of a cracked Jeffcott rotor by means of passing its critical speed and sub-harmonic resonance have been carried out by Darpe et al. [7]. It is shown that the breathing behaviour and the peak response are strongly influenced by the unbalance orientation angle. In separate work, Darpe et al. [8] presented a novel way to detect fatigue transverse cracks in rotating shafts. In this technique, transient torsional excitation has been applied for a very short duration at a specific angular orientation of the rotor, and by using wavelet transform, the transient features of the resonant bending vibration have been revealed. A good feature of their proposed method is that the response features are not similar to the responses of other common rotor faults under similar excitation. Patel et al. [9] investigated the influence of crack breathing models on the nonlinear vibration characteristics of cracked rotors. Using two crack models, that is, a switching crack model and response-dependent breathing crack model, the dynamic responses for both the crack models are compared.

In comparison with transverse cracks, there are very few investigations into slant cracks. In this way, a qualitative analysis of the transverse vibration of a rotor system with a crack at an angle of 45 degrees toward the axis of the shaft has been presented by Ichimonji [10]. Based on some assumptions, the equation of motion of a simple rotor system with a slant crack is derived. The equation of motion has been represented by a differential equation with parametric excitation in the coordinate system rotating at the operating speed of the rotor. It was concluded that the steady state transverse response of the rotor system contains peaks at the operating speed, twice that of the operating speed and their sub-harmonic frequencies. The transverse vibration of a rotor system with a slant crack under torsional vibration has also been investigated in [11]. The transverse vibration of the rotor was considered to be closely related to the torsional vibration. Sekhar et al. [12] conducted a finite element (FEM) analysis of a rotor-bearing system with slant crack. It was concluded that the steady state response of the cracked rotor was found to have sub-harmonic frequency components at an interval frequency corresponding to the torsional frequency. An analysis of vibration characteristics of a slant cracked rotor passing through its flexural critical speed using a finite element method is carried out by Sekhar et al. [13]. The transient response of a cracked rotor has been investigated, and it was concluded that when a crack is present in the rotor, the sub- and super-harmonic frequency components, at an interval frequency corresponding to the torsional frequency, are found to be centred on the critical speed of the rotor system. A comparison of the influence of transverse crack and slant one on the response of a rotor system is presented by Sekhar et al. [14]. They concluded that the vibration behaviour of a rotor with a slant crack is less sensitive to mechanical impedance. It is shown that breathing in slant cracks also depends on the torsional excitation frequency. Darpe [15] presented a simple Jeffcott rotor model of a rotor with a slant crack. A flexibility matrix of the rotor with a slant crack has been developed, and the stiffness coefficients based on the flexibility values have been used in the equations of motion. It is observed that a rotor with a slant crack is stiffer in the lateral and longitudinal directions, but more flexible in torsion, compared to a rotor with a transverse crack. In addition, the responses of rotors with two types of cracks (i.e. transverse and slant) at sub-harmonic resonances have been investigated. In a further paper [16], he presented a finite element model for a rotor with a slant crack. The comparison between the rotor with slant and transverse cracks has been made with respect to the stiffness coefficients and coupled vibration response characteristics. It is shown that the stiffness matrix for slant cracks is more populated with additional cross-coupled coefficients.

Bachschmid et al. [17], using 3D FEM, investigated the breathing mechanism in a rotating shaft. Slant and helicoidal cracks are the two types of crack shape models that they considered. A simplified model to determine the open area of the crack is also presented in their work which has then been used for analysing the nonlinear dynamic behaviour of cracked rotating shafts, which occurs when breathing is governed by the vibration itself.

Papadopoulos [18] in his excellent review paper explained many crack models, such as open crack, switching crack, second moment inertia, breathing and harmonic model approaches. Strain energy release rate theory (SERR) and its combination with linear fracture mechanics and rotor dynamics have been considered in detail

for calculating the compliance matrix. Lin et al. [19] investigated the dynamic behaviour of a slant (45° crack angle) cracked rotor. Using the Jeffcott rotor model, the equation of motion was extracted in four directions. They mentioned that it requires a much longer time to compute the steady responses of a breathing cracked shaft than that of an open cracked shaft, and therefore, almost all the investigation in their paper adopted an open crack model. It is stated that the existence of the frequency of torsional excitation in the longitudinal response and the combined frequencies of the rotating frequency and the frequency of torsional excitation in the transverse response are good identifiers for slant crack detection.

To the best knowledge of the authors, few studies on rotors with slant cracks are reported. This is the main reason for this study. A cracked Jeffcott rotor with a slant crack on the shaft was considered, and the element of the flexibility matrix (and there for stiffness matrix) of the system was calculated. Also, the influence of crack orientations on the flexibility coefficients and subsequently on the amplitude of the frequency responses in several prominent frequencies is investigated.

The outline of the paper is as follows. Equations of the motion of a cracked Jeffcott rotor system are derived in Sect. 2. The elements of the flexibility matrix of the system are given in Sect. 3. Using numerical illustrations, vibration behaviour of the system under arbitrary crack orientation angles are shown and analysed in Sect. 4. Based on the study considered in this paper, a set of conclusions are presented in Sect. 5.

2 Equations of motion

Consider a Jeffcott rotor rotating at speed Ω (Fig. 1). The shaft is assumed to be massless, and a disk of mass m is placed in the middle of the shaft. A view of cross-section of the disk is shown in Fig. 2. In this figure, XOY is the stationary coordinate, $\xi o \eta$ is the rotational coordinate with centre o, and $\xi' o' \eta'$ is rotational coordinate that is attached to the centre of the disk. Point o' is the centre of the disk, c is the disk's centre of mass, α is the angle representing the torsional vibration of the system, and φ is the phase angle of the centre of mass.

The angle position of the centre of mass is given by

$$\theta = \Omega t + \alpha + \varphi \tag{1}$$

Using the d'Alambert principle (Fig. 3), the equation of the motion in four directions (two transverse, one torsional and one longitudinal) can be established as

$$\begin{aligned} m\ddot{x} + c\dot{x} + k_x x + k_{xy} y + k_{xT}\alpha + k_{xu} u &= -\mathrm{mg} + \mathrm{me}(\Omega + \dot{\alpha})^2 \cos(\Omega t + \alpha + \varphi) \\ &\quad + \mathrm{me}\ddot{\alpha} \sin(\Omega t + \alpha + \varphi) \qquad (2) \\ m\ddot{y} + \mathrm{c}\dot{y} + k_{xy} x + k_y y + k_{yT}\alpha + k_{yu} u &= \mathrm{me}(\Omega + \dot{\alpha})^2 \sin(\Omega t + \alpha + \varphi) \\ &\quad - \mathrm{me}\ddot{\alpha} \cos(\Omega t + \alpha + \varphi) \qquad (3) \\ J\ddot{\alpha} + c_T(\Omega + \dot{\alpha}) + k_{xT} x + k_{yT} y + k_T \alpha + k_{Tu} u &= M(t) + \mathrm{mge} \sin(\Omega t + \alpha + \varphi) \end{aligned}$$

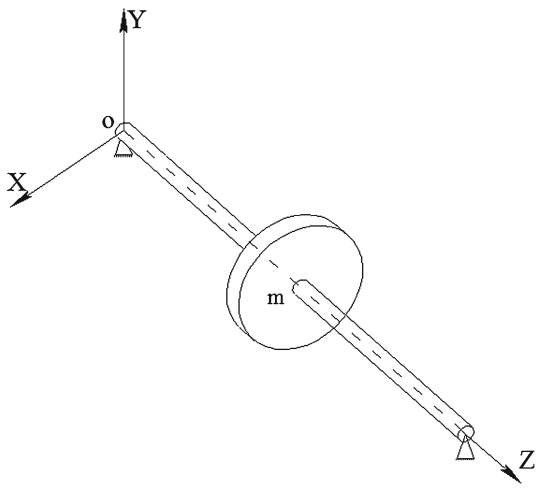

Fig. 1 Jeffcott rotor model

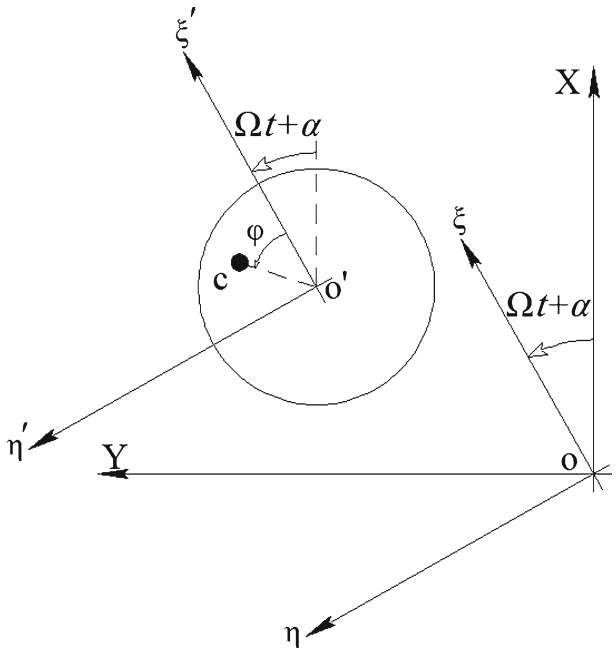

Fig. 2 Cross-sectional view of crack at centre point of the shaft

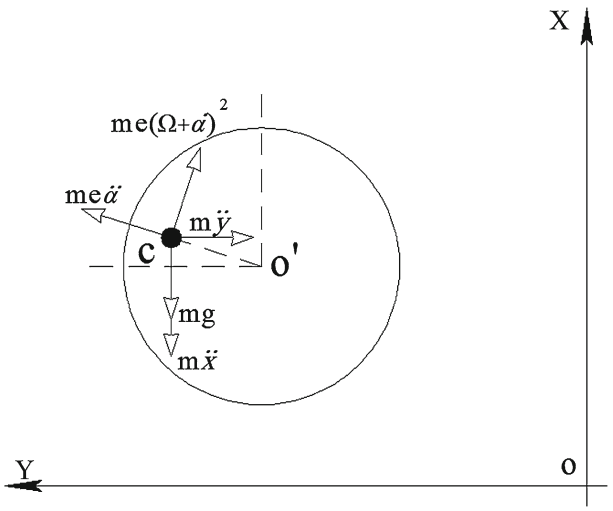

Fig. 3 Forces exerted on the centre of mass of the disk

$$+\mathrm{me}\ddot{x}\sin(\Omega t+\alpha+\varphi)-m\ddot{y}e\cos(\Omega t+\alpha+\varphi) \quad (4)$$

$$m\ddot{u}+c_u\dot{u}+k_{xu}x+k_{yu}y+k_{Tu}\alpha+k_u u=0 \quad (5)$$

where J is the mass moment of inertia of the disk about o'; c, c_T and c_u are the damping coefficients in the transverse, torsional and longitudinal directions. It should be mentioned that these equations are the same as those reported in [19]. Furthermore, $M(t)$ is the torsional excitation and e is the eccentricity of the disk. Using Eqs. (3)–(6), the stiffness matrix of the system can be determined as

$$\mathbf{K_g}=\begin{bmatrix} k_x & k_{xy} & k_{xT} & k_{xu} \\ k_{xy} & k_y & k_{yT} & k_{yu} \\ k_{xT} & k_{yT} & k_T & k_{Tu} \\ k_{xu} & k_{yu} & k_{Tu} & k_u \end{bmatrix} \quad (6)$$

The existence of a crack, which in this paper is located in the mid-span of the shaft, can affect the elements of this matrix. This will be shown in the following sections.

3 Flexibility matrix of a rotor with slant crack

In this section, using the strain energy release rate method and Castigliano's theorem, the crack compliance matrix is calculated. It is known that the total strain energy of a cracked shaft is the sum of the strain energy of the un-cracked shaft and strain energy caused by the crack, and according to Fig. 4, which shows a cracked shaft under four external loads, the total strain energy is

$$E_{\text{total}} = U_{\text{uncarcked shaft}} + W_{\text{cracked shaft}} = \frac{F_x^2 l^3}{96\text{EI}} + \frac{F_y^2 l^3}{96\text{EI}} + \frac{T^2 l}{4\text{GJ}} + \frac{F_z^2 l}{4\text{AE}} \tag{7}$$

where G is the shear modulus, and A is the cross-sectional area of the shaft.

Supposing that the internal reactions on an element of a shaft containing a crack are two bending moments q_4 and q_5, one torsional moment T and one longitudinal force q_1 (Fig. 5),

$$W = W(q_5, q_4, T, q_1). \tag{8}$$

According to Eqs. (7) and (8) and also by using Castigliano's theorem, the local flexibility of the cracked shaft is

$$\frac{\partial^2 E}{\partial F_i \partial F_j} = \frac{\partial^2 U}{\partial F_i \partial F_j} + \frac{\partial^2 W}{\partial F_i \partial F_j} \tag{9}$$

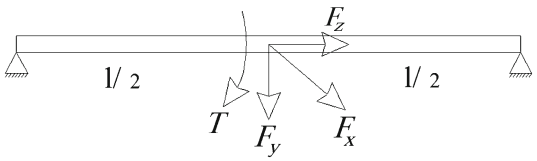

Fig. 4 A cracked shaft under external loads

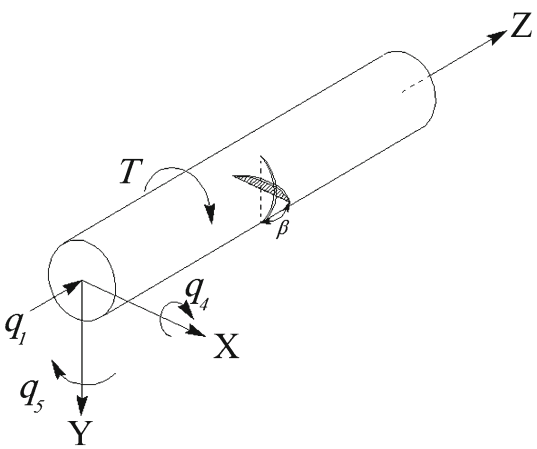

Fig. 5 Internal reactions on the crack

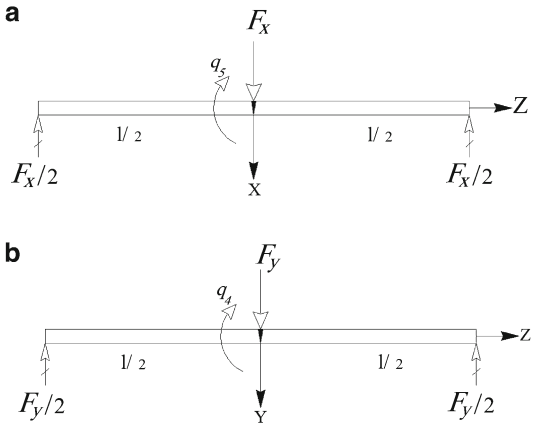

Fig. 6 Relation between external and internal loads: **a** between F_x and q_5, **b** between F_y and q_4

Using Eq. (9) and $q_4 = F_y l/4$, $q_5 = F_x l/4$ (from Fig. 6a, b), the flexibility matrix of a cracked shaft C_l can be written as (see "Appendix")

$$\mathbf{C_l} = \begin{bmatrix} \frac{l^2}{16}\left(\frac{\partial^2 W}{\partial q_5^2}\right) + \frac{l^3}{48\mathrm{EI}} & \frac{l^2}{16}\left(\frac{\partial^2 W}{\partial q_5 \partial q_4}\right) & \frac{l}{4}\left(\frac{\partial^2 W}{\partial q_5 \partial T}\right) & \frac{l}{4}\left(\frac{\partial^2 W}{\partial q_5 \partial q_1}\right) \\ & \frac{l^2}{16}\left(\frac{\partial^2 W}{\partial q_4^2}\right) + \frac{l^3}{48\mathrm{EI}} & \frac{l}{4}\left(\frac{\partial^2 W}{\partial q_4 \partial T}\right) & \frac{l}{4}\left(\frac{\partial^2 W}{\partial q_4 \partial q_1}\right) \\ & & \frac{\partial^2 W}{\partial T^2} + \frac{l}{2\mathrm{GJ}} & \frac{\partial^2 W}{\partial q_1 \partial T} \\ \text{sym.} & & & \frac{\partial^2 W}{\partial q_1^2} + \frac{l}{2\mathrm{AE}} \end{bmatrix} = \mathbf{G}_1 \times \mathbf{\Delta} c_{ij} \times \mathbf{G}_2 + \mathbf{C_s} \quad (10)$$

where

$$\mathbf{\Delta c}_{ij} = \frac{\partial^2 W}{\partial q_i \partial q_j}, \mathbf{G}_1 = \left[\frac{1}{4}, \frac{1}{4}, 1, 1\right], \mathbf{G}_2 = \left[\frac{1}{4}, \frac{1}{4}, 1, 1\right], \mathbf{C}_s = \mathrm{diag}\left(\frac{\mathrm{l}^3}{48\mathrm{EI}}, \frac{\mathrm{l}^3}{48\mathrm{EI}}, \frac{1}{2\mathrm{GJ}}, \frac{1}{2\mathrm{AE}}\right) \quad (11)$$

It is obvious that Eq. (10) leads to a symmetric matrix, whereas some researchers reported that it had a nonsymmetric form [18–20].

It should be mentioned that symmetric forms that are presented in [12–16] have been used for FE method, while relation (11) and those are presented in [18–20] are used for analytic method. Using fracture mechanics theory, the strain energy due to the presence of a crack on the shaft can be expressed as

$$W = \int_A J(A)dA = \int_A \frac{1}{\mathrm{E}'}\left[K_{\mathrm{I}}^2 + (1+\nu)K_{\mathrm{III}}^2\right]dA = \int_{A\prime} \frac{1}{\mathrm{E}'}K_{\mathrm{I}}^2 dA' + \int_A \frac{1}{\mathrm{E'}}(1+\nu)K_{\mathrm{III}}^2 dA \quad (12)$$

where $J(A)$ is the strain energy density function. In general, $J(A)$ is a function of K_{I}, K_{II} and K_{III}, which are the stress intensity factors for opening, sliding and tearing modes, respectively. Also, ν is the Poisson's ratio and $E' = E/1 - \nu^2$. As is shown in Eq. (12), for the tearing mode, the total surface of the crack, that is, A, is used for integration, while for the opening mode, part of the crack surface which remains open during rotation $A\prime$ should be taken into account [19].

The crack surface at θ orientation is shown in Fig. 7. According to this figure, the stress intensity factors for a slant crack at θ angle are tabulated in Table 1 where $x_0 = \eta_0 \sin(\theta)$.

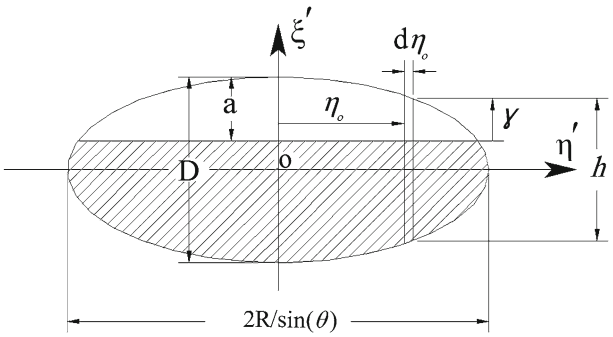

Fig. 7 Crack surface at θ orientation

Table 1 Stress intensity factors for a slant crack at θ angle

Caused by	K_{I}	K_{III}
q_1 :	$K_{\mathrm{I}}^1 = \frac{q_1}{\pi R^2}\sin^2(\theta)\sqrt{\pi\gamma}F_1$,	$K_{\mathrm{III}}^1 = \frac{q_1}{\pi R^2}\sin(\theta)\cos(\theta)\sqrt{\pi\gamma}F_{\mathrm{III}}$.
q_4 :	$K_{\mathrm{I}}^4 = \frac{4q_4x_0}{\pi R^4}\sin^2(\theta)\sqrt{\pi\gamma}F_1$	$K_{\mathrm{III}}^4 = \frac{2q_4x_0}{\pi R^4}\sin(\theta)\cos(\theta)\sqrt{\pi\gamma}F_{\mathrm{III}}$
q_5 :	$K_{\mathrm{I}}^5 = \frac{4q_5\sqrt{R^2-x_0^2}}{\pi R^4}\sin^2(\theta)\sqrt{\pi\gamma}F_2$	$K_{\mathrm{III}}^5 = \frac{2q_5}{\pi R^4}\sin(2\theta)\sqrt{\pi\gamma}F_{\mathrm{III}}$
T :	$K_{\mathrm{I}}^T = \frac{2T\sqrt{R^2-x_0^2}}{\pi R^4}\sin(2\theta)\sqrt{\pi\gamma}F_2$	$K_{\mathrm{III}}^T = \frac{-2T\sqrt{R^2-x_0^2}}{\pi R^4}\cos(2\theta)\sqrt{\pi\gamma}F_{\mathrm{III}}$

According to [21],

$$F_1 = \sqrt{\frac{\tan(\lambda)}{\lambda}}\left[0.752 + 1.01\frac{\gamma}{\sqrt{\mathrm{R}^2 - x_o^2}} + 0.37(1-\sin(\lambda))^3\right]\frac{1}{\cos(\lambda)},$$
$$F_2 = \sqrt{\frac{\tan(\lambda)}{\lambda}}\left[0.923 + 0.199(1-\sin(\lambda))^4\right]\frac{1}{\cos(\lambda)},$$
$$F_{\mathrm{III}} = \sqrt{\frac{\tan(\lambda)}{\lambda}}, \lambda = \frac{\pi\gamma}{4\sqrt{R^2 - x_o^2}} \tag{13}$$

Therefore, the total strain density functions are

$$K_{\mathrm{I}} = \left(\frac{q_1}{\pi R^2}\sin^2(\theta)F_1 + \frac{4q_4x_0}{\pi R^4}\sin^2(\theta)F_1 + \frac{4q_5\sqrt{R^2-x_0^2}}{\pi R^4}\sin^2(\theta)F_2 + \frac{2T\sqrt{R^2-x_0^2}}{\pi R^4}\sin(2\theta)F_2\right)\sqrt{\pi\gamma} \tag{14}$$

$$K_{\mathrm{III}} = \left(\frac{q_1}{\pi R^2}\sin(\theta)\cos(\theta) + \frac{2q_5}{\pi R^4}\sin(2\theta) - \frac{2T\sqrt{R^2-x_0^2}}{\pi R^4}\cos(2\theta)\right)\sqrt{\pi\gamma}F_{\mathrm{III}} \tag{15}$$

Thus, by using Eqs. (13), (14) and (15), the total strain energy is known. It should be noticed that K_{III}^T (Table 1) appeared in different form in the literature [6,15].

After calculating the local flexibility of a cracked rotor, the local stiffness of the system can be calculated.

$$\mathbf{K_l} = \mathbf{C_l}^{-1} \tag{16}$$

The global stiffness matrix in the inertial coordinate system is

$$\mathbf{K_g} = \mathbf{H}^{-1} \times \mathbf{K_l} \times \mathbf{H}, \mathbf{H} = \begin{bmatrix} \cos(\Omega t+\alpha) & \sin(\Omega t+\alpha) & 0 & 0 \\ -\sin(\Omega t+\alpha) & \cos(\Omega t+\alpha) & 0 & 0 \\ 0 & 0 & 1 & 0 \\ 0 & 0 & 0 & 1 \end{bmatrix} \tag{17}$$

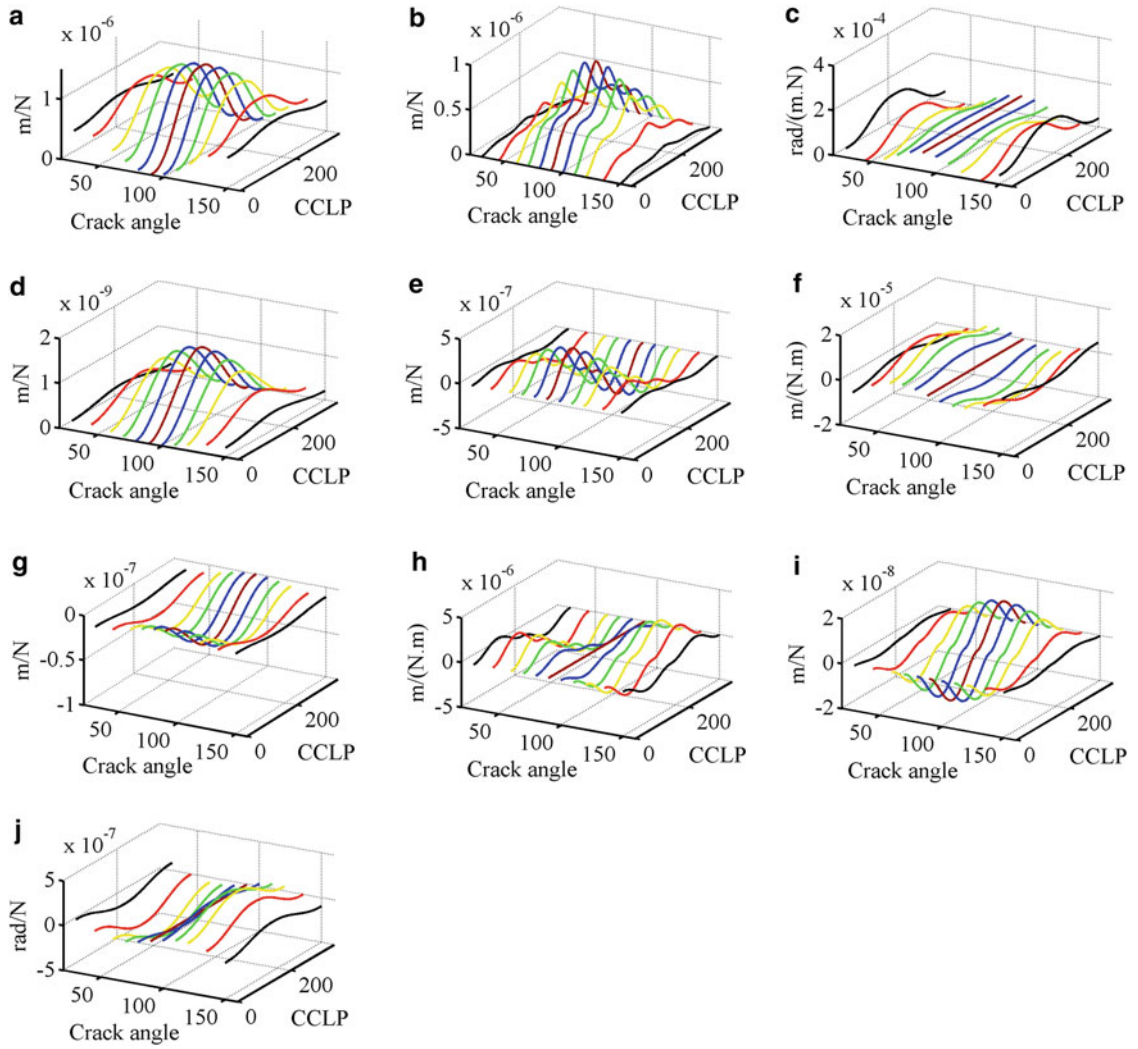

Fig. 8 Variation in the elements of local flexibility matrix versus CCLP and crack orientation from 30° to 90°, **a** c(1,1), **b** c(2,2), **c** c(3,3), **d** c(4,4), **e** c(1,2), **f** c(1,3), **g** c(1,4), **h** c(2,3), **i** c(2,4), **j** c(3,4)

For a 9.5 mm diameter shaft with a crack depth equal to its radius, the elements of the local flexibility matrix are evaluated for different crack orientations from 30° to 150°. In Fig. 8, the variations in these flexibilities versus CCLP[1] [6] and crack orientations (30°, 45°, 60°, 70°, 80°, 90°, 100°, 110°, 120°, 135° and 150°) are shown.

It should be mentioned that the crack tip is divided into 360 points in order to use the CCLP method; therefore, CCLP = 180 expresses that the crack is fully open, and CCLP = 0 or 360 identifies a fully closed crack. According to Fig. 8, any increase in the value of the crack angle from 30° to 90° increases the maximum value of $c(1, 1)$ and $c(2, 2)$. However, any increase in the crack angle from 90° to 150° decreases the maximum value of these coefficients. It should be mentioned that the maximum value of these coefficients occurs when the crack is fully open (CCLP = 180). In bending, if the crack is fully open, the transverse crack is more flexible than the slant crack and the larger the crack angle, the greater the flexibility. There is a difference between the variation in $c(1, 1)$ and $c(2, 2)$. When the crack is fully closed, the values of $c(1, 1)$ for a slant crack are more than that of a transverse one. However, there is no difference between the values of $c(2, 2)$ for slant or transverse cracks. For a fully open crack, the magnitude of $c(3, 3)$ for a slant crack is greater than the transverse one. This indicates that in torsion, the slant crack is more flexible than the transverse crack. Similar results are also reported in [15]. It should be mentioned that for a fully closed crack, a slant crack with a 45° orientation angle has no flexibility components in torsion.

[1] Crack closure line position.

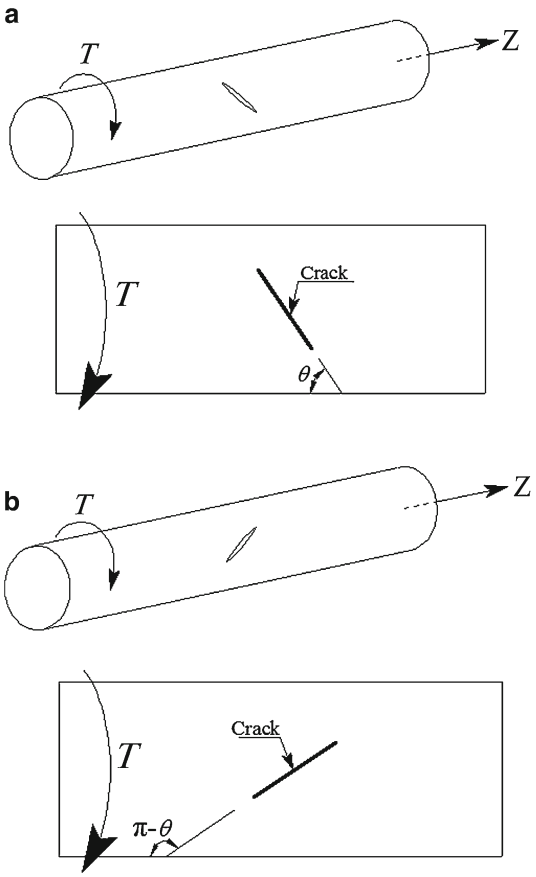

Fig. 9 Different crack orientation angles, **a** θ type *slant crack*, **b** $\pi - \theta$ type *slant crack*

Among slant cracks with different orientations, the 45° slant crack has the minimum value in torsion. The reason is that, according to K_{III}^{T} from Table 1, when θ is $\pi/2$, the stress intensity factor in the 3rd mode that is caused by T is zero. It should be noted that the value of the $c(3, 3)$ coefficient for a transverse crack is not sensitive to the area of the open part of the crack. In other words, the value of $c(3, 3)$ does not depend on the value of CCLP. Coefficients $c(4, 4)$ and $c(1, 4)$ have similar trends to each other. From Fig. 8, it can be seen that $c(1, 3)$, $c(2, 3)$ and $c(3, 4)$ are zero for transverse cracks. This means that the effects of coupling for slant cracks are more considerable than that in transverse cracks. In this paper, if the crack angle is less than 90°, it is called a "slant crack with θ angle", and if the crack angle is greater than 90°, it is called a "slant crack with $\pi - \theta$ angle". The type of slant crack is dependent on the rotor whirl direction. Fig. 9 illustrates θ and $\pi - \theta$ slant cracks in a shaft.

From Fig. 8, it is obvious that only the coefficients of $c(1, 3)$, $c(2, 3)$ and $c(3, 4)$ are different for θ and $\pi - \theta$ in a slant crack. For example, according to Fig. 8, the value of $c(1, 3)$ for a slant crack of 30° and 150° is equal in magnitude but different in sign. Due to the symmetry of the local flexibility matrix, the coefficients $c(3, 1)$, $c(3, 2)$ and $c(4, 3)$ have opposite signs for slant cracks of θ and $\pi - \theta$. Therefore, all coefficients in the 3rd row and the 3rd column of the local flexibility matrix are different for slant cracks of θ and $\pi - \theta$ except $c(3, 3)$. An explanation is presented here using Mohr's circle. Figure 10a shows elements E1 and E2 on a cracked shaft. Based on Fig. 13a, if element E1 rotates β degrees counterclockwise, it will coincide with E2 (Fig. 10b).The Mohr's circle for element stresses is presented in Fig. 10c.

From the Mohr's circle, the axial and shear stresses on element E2 can be calculated. According to this figure, when the shaft has a slant crack with an angle of θ, the axial tension stress of σ_1' is exerted on the surface of crack and causes the crack surfaces to separate from each other. However, for slant cracks with angle of $\pi - \theta$, the compression stresses of σ_2' exist on the surface of the crack and will close it (Fig. 11). Therefore, it can be concluded that two types of slant crack do not experience the same stress fields. As already mentioned, the magnitude of σ_1' and σ_2' is equal but is different in sign. On the other hand, the stress intensity

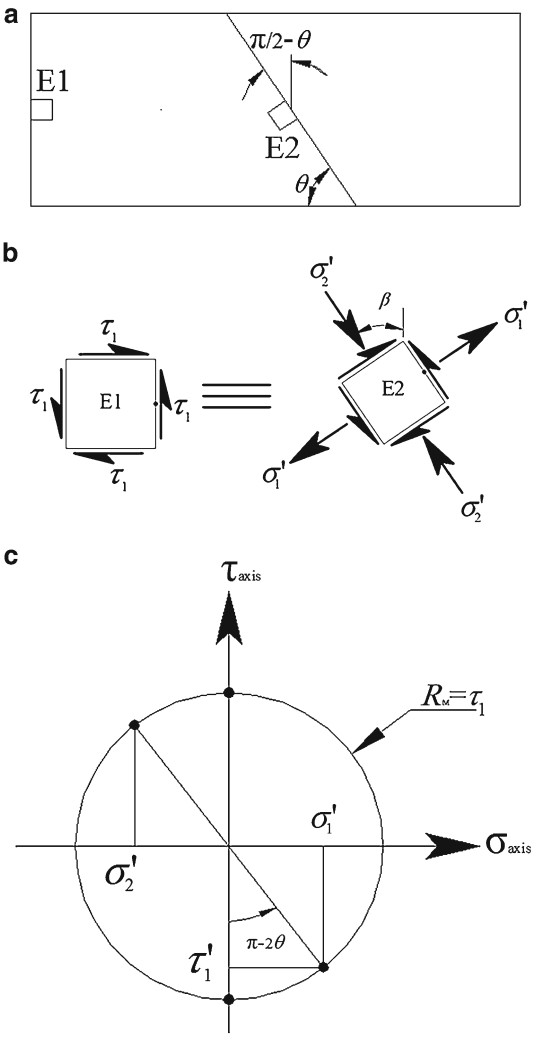

Fig. 10 **a** E1 and E2 elements, **b** E1 and E2 elements after β rotation (CCW), **c** Mohr's circle

factors depend on the stresses that are exerted on the crack surfaces. This is why there is difference between the coefficients that are generated from T (i.e. coefficients in the 3rd row and 3rd column).

4 Vibration response of rotor system with slant crack

The parameters that are required for solving the equations of motion are summarized in Table 2.

Solving the equations of motion for a breathing crack is very time-consuming in comparison with an open crack model. On the other hand, the same prominent characteristic frequencies exist for these two models [19]. Therefore, all investigations in this paper are carried out for open cracks. The Runge–Kutta method is used for solving the equations of motion. Using this method, the response of a Jeffcott rotor with a slant crack under different crack angles is evaluated.

In Figs. 12, 13, 14, the spectrum of transverse, torsional and longitudinal responses (respectively) of a cracked shaft with θ slant crack and its complementary angle of slant crack is compared. The crack is open and its depth is equal to radius of the shaft.

According to Fig. 12a, the difference between the spectrum of transverse responses for 30° and 150° slant cracks can be seen in $\Omega, \Omega + \omega_{\mathrm{T}}$ and 3Ω frequencies. In Ω and $\Omega + \omega_T$, the amplitude of the response of a 30° slant crack is larger than that of 150°. Generally, in the response of other angles (45°, 60°, 70°, 80°, 100°, 110°, 120° and 135°), the differences can be seen in the frequencies $\Omega, 2\Omega \pm \omega_{\mathrm{T}}$

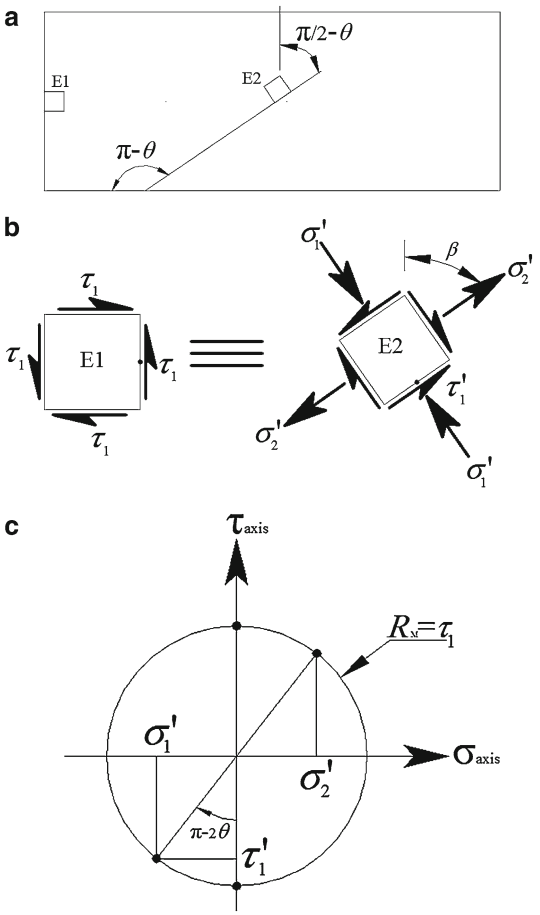

Fig. 11 **a** E1 and E2 elements, **b** E1 and E2 element after β rotation (CW), **c** Mohr's circle

Table 2 Characteristics of the studied rotor system

Speed of revolution	$\Omega = 500$ rpm	Disk mass	$m = 0.595$ kg
Torsional excitation freq.	$\omega_T = 0.6\Omega = 300$ rpm	Shaft length	$l = 0.26$ m
External torsional excitation	$M_T = \sin(\omega_T t)$	Shaft diameter	$D = 9.5$ mm
Transverse damp coefficient	$c = 41.65$ kg/s	Disk diameter	dp $= 76$ mm
Torsional damp coefficient	$c_T = 0.0091$ kg.m^2/s	Initial phase angle	$\varphi = \pi/6$rad
Longitudinal damp coefficient	$c_u = 146.2034$ kg/s	Poisson's ratio	$\nu = 0.3$
Modulus of elasticity	$E = 210$ Gpa	Eccentricity	$e = 0.1643$ mm

and 3Ω. For these angles, in the Ω and $2\Omega - \omega_T$ frequencies, the amplitude of the transverse response of $\pi - \theta$ slant cracks is larger than the amplitude of the response of θ slant cracks, while a reverse trend is observable for the other frequencies ($2\Omega + \omega_T$ and 3Ω).

It can be concluded that at the Ω frequency, if there is difference between the amplitude of the transverse spectrums of θ slant cracks and its complementary angle slant cracks for the CW[2] whirl and CCW[3] whirl, respectively, the existence of a slant crack on the shaft is more probable. In other words, the change in the flexibility of a slant cracked shaft in CW and CCW rotation results in a difference in the amplitude of the spectrum of the response for these two kinds of whirl.

It is significant that the general schemas of the spectrums of 30° and 150° slant cracks are not completely the same and that they have sensible difference in comparison with spectrums of other angles. According to Fig. 8, the reason is that there are three coefficients ($c(1, 3)$, $c(2, 3)$ and $c(3, 4)$) in the flexibility matrix that can cause coupling between the torsional direction and other directions. The coefficient $c(2, 3)$ is zero for all

[2] Clockwise: in this paper, rotation about the symmetry axes of the shaft which closes two edges of the crack.

[3] Counterclockwise: in this paper, rotation about the symmetry axes of the shaft which opens two edges of the crack.

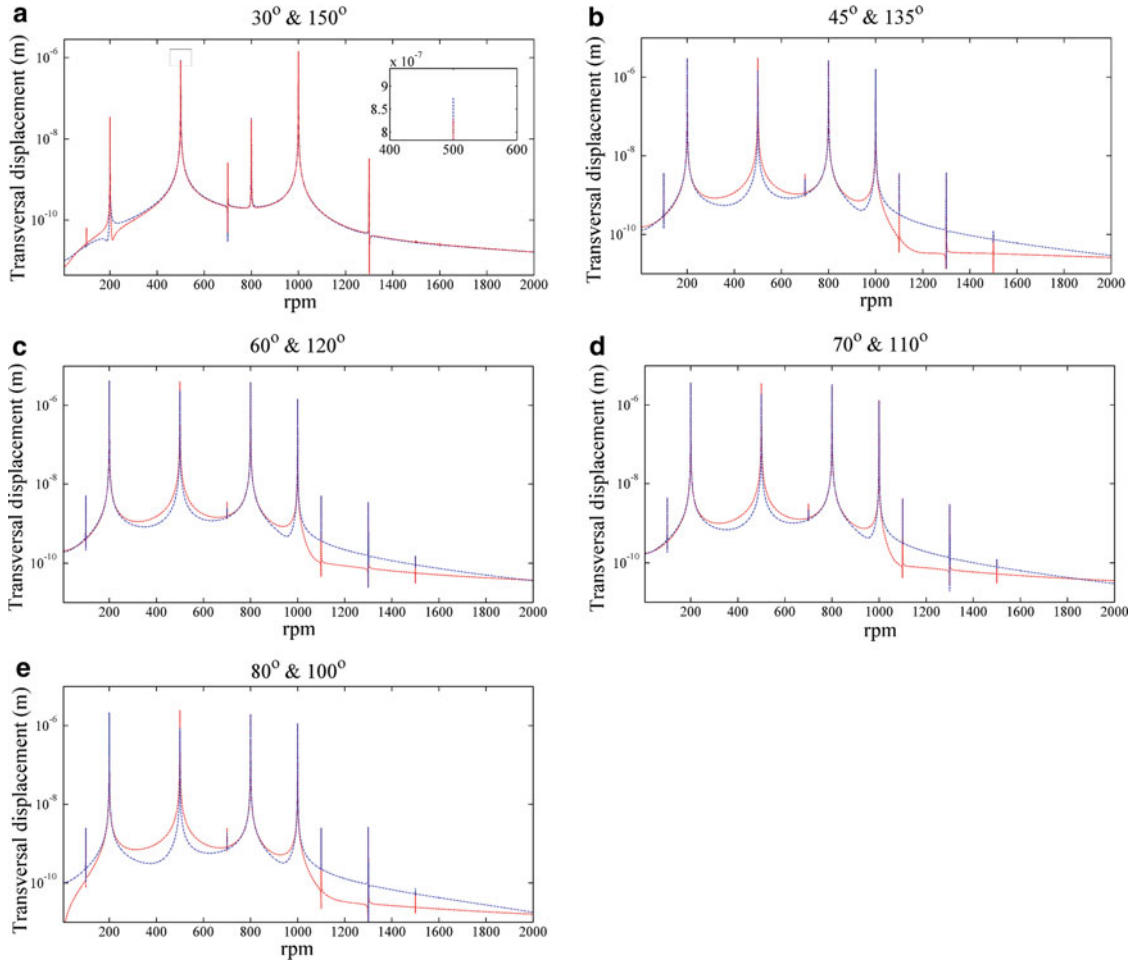

Fig. 12 Comparison between transversal spectrums of *slant crack* with complementary angles (*blue line/dashed point line*: θ *slant crack* & *red line/dashed line* $\pi - \theta$ *slant crack*), **a** 30° and 150° *slant cracks*, **b** 45° and 135° *slant cracks*, **c** 60° and 120° *slant cracks*, **d** 70° and 110° *slant cracks* and **e** 80° and 100° *slant cracks*. (Color figure online)

angles of crack orientation (open crack or CCLP = 180). The effect of coefficient $c(3, 4)$ is also negligible due to the fact that the system does not have any longitudinal motion. Therefore, the only coefficient that can cause coupling between transverse and torsional responses is $c(1, 3)$. On the other hand (according to Fig. 8), the coefficient $c(1, 3)$ is only zero for 30^o and 150° slant cracks. The difference between the spectrums of the transverse responses of a 30° and 150° slant crack with other crack angles is only due to $c(1, 3)$.

It should be noted that the existence of combined frequencies such as $\Omega \pm \omega_T$ and $2\Omega \pm \omega_T$ in the spectrum of transverse responses (for 30° and 150°) is due to the coupling phenomena that are caused by eccentricity (see Eqs. (2), (3) and (4)).

According to Fig. 13, in the spectrum of the torsional response of a shaft with a θ slant crack in comparison with the spectrum of the same response of a shaft with a $\pi - \theta$ slant crack, there is no difference in the amplitude at ω_T frequency. But in other frequencies (i.e. Ω and $\Omega + \omega_T$), the difference is visible. In the frequency of Ω, for angles except 30° and 150°, the amplitude of the torsional response for a $\pi - \theta$ slant crack is greater than the amplitude of the same response for a θ slant crack. However, for 30° and 150° slant cracks, this relation is reversed. In the spectrum of the torsional response for 30° and 150° slant cracks, the frequency $\Omega + \omega_T$ does not exist. For other angles and in the $\Omega + \omega_T$ frequency, the amplitude of the torsional response for θ slant cracks is greater than the amplitude for $\pi - \theta$ slant cracks.

The frequency 2Ω is not seen in the spectrum of longitudinal responses for 30° and 150° slant cracks (Fig. 14a). But in $\Omega \pm \omega_T$ frequencies, the amplitude of the longitudinal response for a 30° slant crack is greater than that of the 150° slant crack. In other angles at frequencies of $\Omega \pm \omega_T$ and 2Ω, the amplitude of the

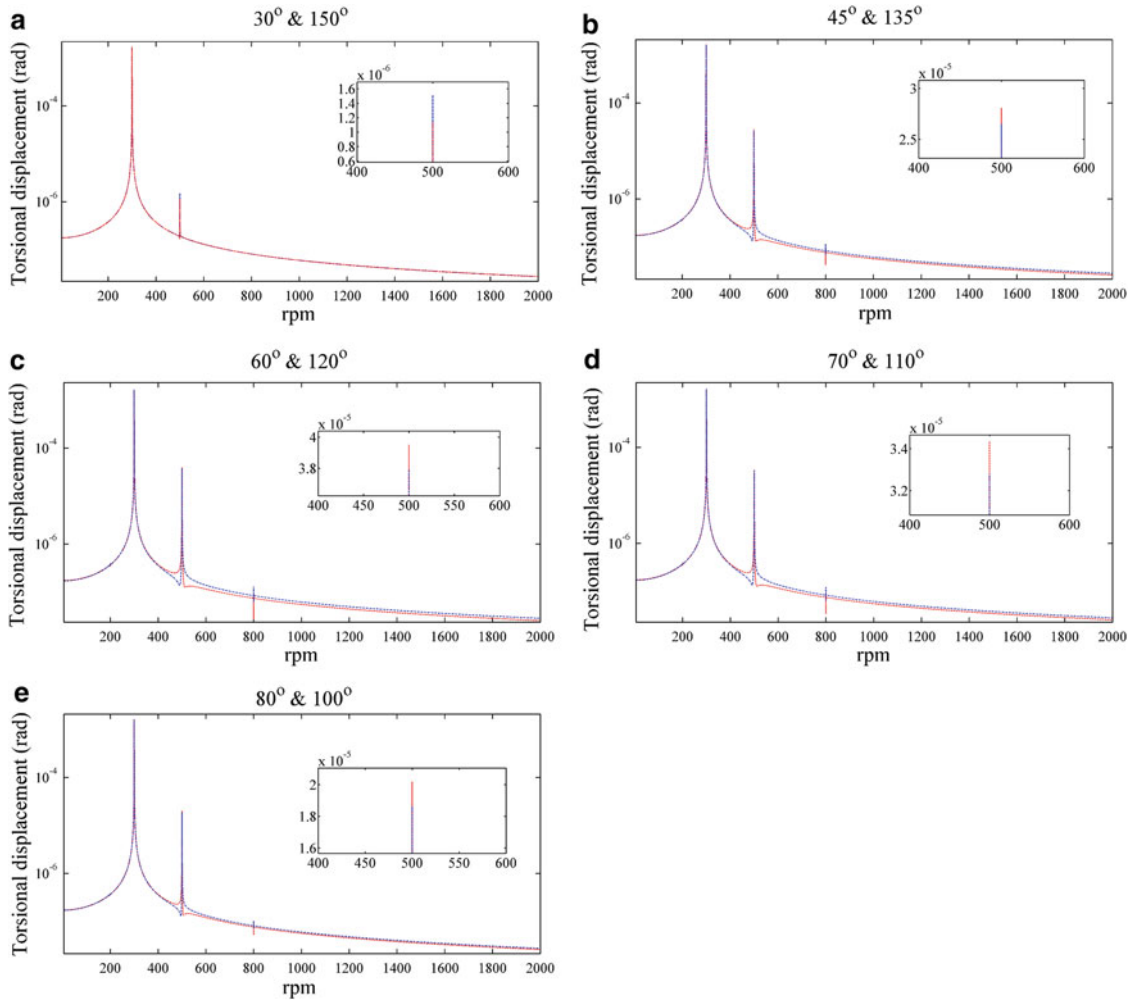

Fig. 13 Comparison between torsional spectrums of *slant crack* with complementary angles (*blue line/ dashed point line*: θ *slant crack* & *red line/ dashed line* $\pi - \theta$ *slant crack*), **a** 30° and 150° *slant cracks*, **b** 45° and 135° *slant cracks*, **c** 60° and 120° *slant cracks*, **d** 70° and 110° *slant cracks* and **e** 80° and 100° *slant cracks*. (Color figure online)

longitudinal responses for θ slant cracks are greater than the amplitude of the same response for $\pi - \theta$ slant cracks.

In conclusion, the spectrum of the responses of the θ slant crack and $\pi - \theta$ in CW and CCW revolutions is not the same, and any difference in response amplitude of a rotor system in CW and CCW directions (especially at the above mentioned frequencies) may lead one to identify the existence of a slant crack on the rotor. Therefore, investigation into the spectrum of the response in forward and backward rotations can be viewed as a good way for slant crack identification in such systems.

5 Conclusion

In this paper, the dynamic behaviour of a Jeffcott rotor system with a slant crack on the shaft is investigated. Only the effects of the crack on the stiffness of the system are considered. Using concepts of fracture mechanics, the flexibility matrix and subsequently the stiffness matrix of the system are evaluated. The formulation was extended for cracks with arbitrary orientation. Variations of the coefficients of the flexibility matrix versus CCLP and crack orientations are shown in some plots and their characteristics are explained. In this paper, two kinds of slant cracks (θ and $\pi - \theta$ slant cracks) are introduced, and it is shown that the coefficients of the 3rd row and 3rd column of the local flexibility matrix for slant cracks with θ and $\pi - \theta$ angles are different.

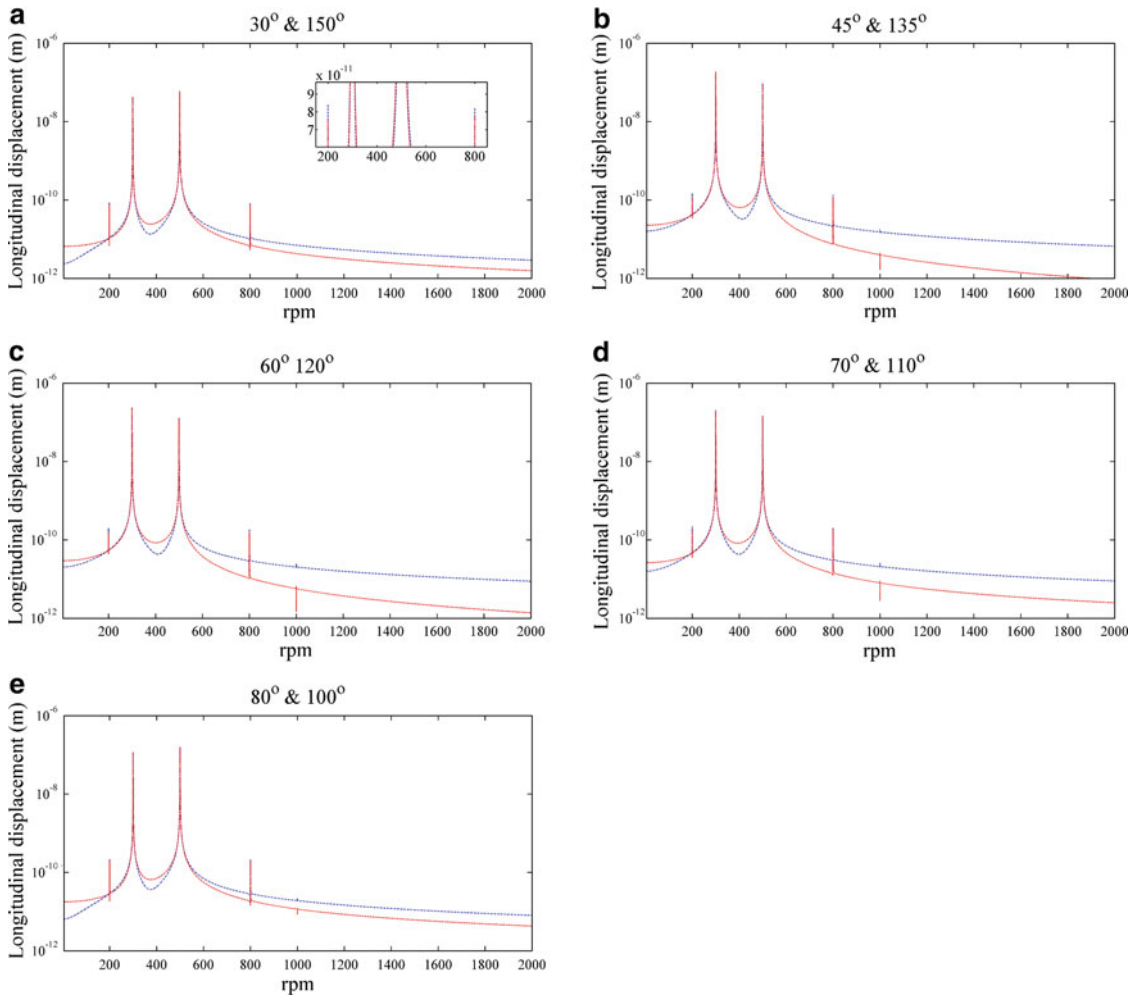

Fig. 14 Comparison between longitudinal spectrums of *slant crack* with complementary angles (*blue line/ dashed point line*: θ *slant crack* & *red line/ dashed line* $\pi - \theta$ *slant crack*), **a** 30° and 150° *slant cracks*, **b** 45° and 135° *slant cracks*, **c** 60° and 120° *slant cracks*, **d** 70° and 110° *slant cracks* and **e** 80° and 100° *slant cracks*. (Color figure online)

Subsequently, using Mohr's circle, it is shown that a slant cracked rotor under CW and CCW rotation has a different compliance matrix.

Assuming an open crack model, the spectrum of the steady response of the system for slant cracks with arbitrary orientation angles is investigated. It is concluded that the spectrum of the responses of the θ and $\pi - \theta$ slant cracks in CW and CCW rotations is not the same. Thus, in order to identify the slant cracks, it is sufficient to compare the spectrums of a rotor system under CW and CCW rotations.

Appendix

Considering Eq. (13) and using chain rule, we have

$$\frac{\partial^2 W}{\partial F_x^2} = \frac{\partial}{\partial F_x}\left(\frac{\partial W}{\partial q_5}.\frac{\partial q_5}{\partial F_x}\right) = \frac{\partial^2 W}{\partial q_5^2}.\left(\frac{\partial q_5}{\partial F_x}\right)^2 + \frac{\partial W}{\partial q_5}.\frac{\partial^2 q_5}{\partial F_x^2} = \frac{\partial^2 W}{\partial q_5^2}.\left(\frac{1}{4}\right)^2 = \frac{1^2}{16}\left(\frac{\partial^2 W}{\partial q_5^2}\right) \quad \text{(A.1)}$$

$$\frac{\partial^2 W}{\partial F_y^2} = \frac{\partial}{\partial F_y}\left(\frac{\partial W}{\partial q_4}.\frac{\partial q_4}{\partial F_y}\right) = \frac{\partial^2 W}{\partial q_4^2}.\left(\frac{\partial q_4}{\partial F_y}\right)^2 + \frac{\partial W}{\partial q_4}.\frac{\partial^2 q_4}{\partial F_y^2} = \frac{1^2}{16}\left(\frac{\partial^2 W}{\partial q_4^2}\right) \quad \text{(A.2)}$$

$$\frac{\partial^2 W}{\partial F_z^2} = \frac{\partial}{\partial F_z}\left(\frac{\partial W}{\partial q_1}.\frac{\partial q_1}{\partial F_z}\right) = \frac{\partial^2 W}{\partial q_1^2}.\left(\frac{\partial q_1}{\partial F_z}\right)^2 + \frac{\partial W}{\partial q_1}.\frac{\partial^2 q_1}{\partial F_z^2} = \frac{\partial^2 W}{\partial q_1^2} \tag{A.3}$$

$$\frac{\partial^2 W}{\partial T^2} = \frac{\partial^2 W}{\partial T^2} \tag{A.4}$$

And,

$$\begin{aligned}\frac{\partial^2 W}{\partial F_x \partial F_y} &= \frac{\partial}{\partial F_x}\left(\frac{\partial W}{\partial q_4}.\frac{\partial q_4}{\partial F_y}\right)\\ &= \frac{\partial^2 W}{\partial q_5 \partial q_4}.\frac{\partial q_5}{\partial F_x}.\frac{\partial q_4}{\partial F_y} + \frac{\partial W}{\partial q_4}.\frac{\partial^2 q_4}{\partial F_x \partial F_y} = \left(\frac{1}{4}\right)\left(\frac{1}{4}\right)\left(\frac{\partial^2 W}{\partial q_5 \partial q_4}\right) = \frac{l^2}{16}\left(\frac{\partial^2 W}{\partial q_5 \partial q_4}\right)\end{aligned} \tag{A.5}$$

$$\frac{\partial^2 W}{\partial F_x \partial F_z} = \frac{\partial}{\partial F_x}\left(\frac{\partial W}{\partial q_1}.\frac{\partial q_1}{\partial F_z}\right) = \frac{\partial^2 W}{\partial q_5 \partial q_1}.\frac{\partial q_5}{\partial F_x}.\frac{\partial q_1}{\partial F_z} + \frac{\partial W}{\partial q_1}.\frac{\partial^2 q_1}{\partial F_x \partial F_z} = \frac{1}{4}\left(\frac{\partial^2 W}{\partial q_5 \partial q_1}\right) \tag{A.6}$$

$$\frac{\partial^2 W}{\partial F_x \partial T} = \frac{\partial}{\partial F_x}\left(\frac{\partial W}{\partial T}\right) = \frac{\partial^2 W}{\partial q_5 \partial T}.\frac{\partial q_5}{\partial F_x} = \frac{1}{4}\left(\frac{\partial^2 W}{\partial q_5 \partial T}\right) \tag{A.7}$$

$$\frac{\partial^2 W}{\partial F_y \partial F_z} = \frac{\partial}{\partial F_y}\left(\frac{\partial W}{\partial q_1}.\frac{\partial q_1}{\partial F_z}\right) = \frac{\partial^2 W}{\partial q_4 \partial q_1}.\frac{\partial q_4}{\partial F_y}.\frac{\partial q_1}{\partial F_z} + \frac{\partial W}{\partial q_1}.\frac{\partial^2 q_1}{\partial F_y \partial F_z} = \frac{1}{4}\left(\frac{\partial^2 W}{\partial q_4 \partial q_1}\right) \tag{A.8}$$

$$\frac{\partial^2 W}{\partial F_y \partial T} = \frac{\partial}{\partial F_y}\left(\frac{\partial W}{\partial T}\right) = \frac{\partial^2 W}{\partial q_4 \partial T}.\frac{\partial q_4}{\partial F_y} = \frac{1}{4}\left(\frac{\partial^2 W}{\partial q_4 \partial T}\right) \tag{A.9}$$

$$\frac{\partial^2 W}{\partial F_z \partial T} = \frac{\partial}{\partial F_z}\left(\frac{\partial W}{\partial T}\right) = \frac{\partial^2 W}{\partial q_1 \partial T}.\frac{\partial q_1}{\partial F_z} = \frac{\partial^2 W}{\partial q_1 \partial T} \tag{A.10}$$

Therefore, according to Eq. (11),

$$\begin{aligned}[c]_l &= \begin{bmatrix} \left(\frac{\partial^2 E}{\partial F_x^2}\right) & \left(\frac{\partial^2 E}{\partial F_x F q_y}\right) & \left(\frac{\partial^2 E}{\partial F_x \partial T}\right) & \left(\frac{\partial^2 E}{\partial F_x \partial F_z}\right) \\ & \left(\frac{\partial^2 E}{\partial F_y^2}\right) & \left(\frac{\partial^2 E}{\partial F_y \partial T}\right) & \left(\frac{\partial^2 E}{\partial F_y \partial F_z}\right) \\ & & \frac{\partial^2 E}{\partial T^2} & \frac{\partial^2 E}{\partial F_z \partial T} \\ sym. & & & \frac{\partial^2 E}{\partial F_z^2} \end{bmatrix}\\ &= \begin{bmatrix} \frac{l^2}{16}\left(\frac{\partial^2 W}{\partial q_5^2}\right) + \frac{l^3}{48EI} & \frac{l^2}{16}\left(\frac{\partial^2 W}{\partial q_5 \partial q_4}\right) & \frac{1}{4}\left(\frac{\partial^2 W}{\partial q_5 \partial T}\right) & \frac{1}{4}\left(\frac{\partial^2 W}{\partial q_5 \partial q_1}\right) \\ & \frac{l^2}{16}\left(\frac{\partial^2 W}{\partial q_4^2}\right) + \frac{l^3}{48EI} & \frac{1}{4}\left(\frac{\partial^2 W}{\partial q_4 \partial T}\right) & \frac{1}{4}\left(\frac{\partial^2 W}{\partial q_4 \partial q_1}\right) \\ & & \frac{\partial^2 W}{\partial T^2} + \frac{1}{2GJ} & \frac{\partial^2 W}{\partial q_1 \partial T} \\ sym. & & & \frac{\partial^2 W}{\partial q_1^2} + \frac{1}{2AE} \end{bmatrix}\end{aligned} \tag{A.11}$$

References

1. Dimarogonas, A.D.: Vibration of cracked structures: a state of the art review. Eng. Fract. Mech. **55**, 831–857 (1996). doi:10.1016/0013-7944(94)00175-8
2. Wauer, J.: On the dynamics of cracked rotors: a literature survey. J. Appl. Mech **43**, 13–17 (1990). doi:10.1115/1.3119157
3. Papadopoulos, C.A., Dimarogonas, A.D.: Coupled longitudinal and bending vibrations of a rotating shaft with an open crack. J. Sound. Vib. **117**, 81–93 (1987). doi:10.1016/0022-460X(87)90437-8
4. Sekhar, A.S.: Vibration characteristics of a cracked rotor with two open cracks. J. Sound. Vib. **223**, 497–512 (1999). doi:10.1006/jsvi.1998.2120
5. Darpe, A.K., Gupta, K., Chawla, A.: Dynamics of a two cracked rotor. J. Sound. Vib. **259**, 649–675 (2003). doi:10.1006/jsvi/2002.5098
6. Darpe, A.K., Gupta, K., Chawla, A.: Coupled bending, longitudinal and torsional vibrations of a cracked rotor. J. Sound. Vib. **269**, 33–60 (2004). doi:10.1016/S0022-460X(03)00003-8

7. Darpe, A.K., Gupta, K., Chawla, A.: Transient response and breathing behaviour of a cracked Jeffcott rotor. J. Sound. Vib. **272**, 207–243 (2004). doi:10.1016/S0022-460X(03)00327-4
8. Darpe, A.K.: A novel way to detect transverse surface crack in a rotating shaft. J. Sound. Vib. **305**, 151–171 (2004). doi:10.1016/jsv.2007.03.070
9. Patel, T.H., Darpe, A.K.: Influence of crack breathing model on nonlinear dynamics of a cracked rotor. J. Sound. Vib. **311**, 953–972 (2008). doi:10.1016/jsv.2007.09.033
10. Ichimonji, M., Watanabe, S.: The dynamics of a rotor system with a shaft having a slant crack. JSME Int. J. **31**, 712–718 (1988)
11. Ichimonji, M., Kazao, S., Watanabe, S., Nonaka, S.: The dynamics of a rotor system with a slant crack under torsional vibration. Nonlinear Stoch. Dyn. **78**, 81–89 (1994)
12. Sekhar, A.S., Balaji Prasad, P.: Dynamics analysis of a rotor system considering a slant crack in the shaft. J. Sound. Vib. **208**, 457–474 (1997). doi:10.1006/jsvi.1997.1222
13. Prabhakar, S., Sekhar, A.S., Mohanty, A.R.: Transient lateral analysis of a slant-cracked rotor passing through its flexural critical speed. Mech. Mach. Theory **37**, 1007–1020 (2002). doi:10.1016/S0094-114X(02)00020-4
14. Sekhar, A.S., Mohanty, A.R., Prabhakar, S.: Vibrations of cracked rotor system: transverse crack versus slant crack. J. Sound. Vib. **279**, 1203–1217 (2005). doi:10.1016/j.jsv.2004.01.011
15. Darpe, A.K.: Dynamics of a Jeffcott rotor with slant crack. J. Sound. Vib. **303**, 1–28 (2007). doi:10.1016/j.jsv.2006.07.052
16. Darpe, A.K.: Coupled vibrations of a rotor with slant crack. J. Sound. Vib. **305**, 172–193 (2007). doi:10.1016/j.jsv.2007.03.079
17. Bachschmid, N., Pennacchi, P., Tanzi, E.: Some remarks on breathing mechanism, on non-linear effects and on slant and helicoidal cracks. Mech. Syst. Signal Process. **22**, 879–904 (2008). doi:10.1016/j.ymssp.2007.11.007
18. Papadopoulos, C.A.: The strain energy release approach for modeling cracks in rotors: a state of the art review. Mech. Syst. Signal Process. **22**, 763–789 (2008). doi:10.1016/j.ymssp.2007.11.009
19. Lin, Y., Chu, F.: The dynamic behavior of a rotor system with a slant crack on the shaft. Mech. Syst. Signal Process. **24**, 522–545 (2010). doi:10.1016/j.ymssp.2009.05.021
20. Papadopoulos, C.A., Dimarogonas, A.D.: Stability of cracked rotors in the coupled vibration mode. J. Vib. Acoust. **110**, 356–359 (1988)
21. Tada, H., Paris, P.C., Irwin, G.R.: The Stress Analysis of Cracks. Professional Engineering Publishing, (2000)